**Superalloys 2004**
*Edited by K.A. Green, T.M. Pollock, H. Harada,*
*T.E. Howson, R.C. Reed, J.J. Schirra, and S. Walston*
***TMS (The Minerals, Metals & Materials Society), 2004***

# CRYSTALLOGRAPHIC INITIATION OF NICKEL-BASE SUPERALLOY IN100 AT RT AND 538°C UNDER LOW CYCLE FATIGUE CONDITIONS

K. Li†, N.E. Ashbaugh†, and A.H. Rosenberger
Air Force Research Laboratory, Material & Manufacturing Directorate, AFRL/MLLMN,
Wright-Patterson AFB, OH 45433-7817, USA
†University of Dayton Research Institute, 300 College Park, Dayton, OH 45469-0128, USA

Keywords: Nickel-base superalloy, crystallographic plane, crack initiation, LCF, OIM

## Abstract

The crystallographic plane of IN100 at the initiation region of fracture surfaces under low cycle fatigue (LCF) conditions at RT and elevated temperature was identified. At RT fatigue cracks initiated on the {111} plane and at elevated temperature on the {001} plane. The initiation plane index was initially determined by investigating the γ′ shape in the γ matrix of fracture surfaces around crack initiation sites and finally verified by orientation image microscopy (OIM). An OIM scan on a sample of original material indicated that local texture might promote a fatigue crack to reach a critical crack size.

## Introduction

Fatigue crack growth mechanisms for nickel-base superalloys are reported to be different for different crack-tip stress intensity factor ranges, ΔK [1]. The fracture mechanism at near threshold and lower portion of the Paris regime appeared to be a highly crystallographic and faceted mode [1-6]. Fatigue crack growth along {111} slip plane or {100} fracture plane was both reported at room temperature and elevated temperature. The actual crack path, whether along {001} or {111} crystallographic plane during fatigue crack propagation, seems to depend on temperature and crack propagation rate, da/dN [1-6]. At RT the faceted crack growth is related to slip band cracking on {111} planes in the crack tip plastic zone [1]. Table 1 summarizes some other reported results. These results indicated that at higher da/dN (> $10^{-4}$ mm/cycle) the fracture plane tended to be {100}, independent of temperature [3]. As da/dN was approached the threshold regime (<$10^{-5}$ - $10^{-6}$ mm/cycle), the fracture plane at RT was {111} [2,4] but at elevated temperature it tended to be {001} [2]. King [4] reported that at RT both {111} and {001} were observed in the facet to striation transition regime (da/dN>$10^{-5}$ mm/cycle), but {111} fracture was dominant. In summary it seems that a high stress intensity factor range ΔK or high temperature promote {001} fracture and a low ΔK (close to threshold regime) and RT promote {111} fracture.

Little work has been done regarding fracture plane crystallography in the faceted fatigue crack initiation region under LCF conditions [4,7]. However, determination of the fracture plane orientation is an initial and crucial step to study LCF mechanisms. As it is well known that in the class of PM nickel-base superalloys, LCF life is related to defect population and microstructure [8-10]. The critical microstructural parameters affecting LCF fatigue life are believed to be grain size and grain orientation. Grain orientations of a flat sample containing a surface crack can be determined using OIM. However, it requires the knowledge of fracture plane orientation to determine the driving force, such as Schmid factor, to initiate a crack and subsequentially to promote microcrack propagation.

Generally, the fracture plane orientation can be measured using Laue x-ray diffraction method if the grain size of the structure is very large. However, the grain size is always small for superalloys when manufactured by powder metallurgy. Thus, the use of x-ray to measure the fracture plane orientation is unrealistic. Some authors [3,4] investigate γ′ shape in the γ grain matrix to obtain the γ grain orientation. The coherent γ′ particles resulted from supersolvus temperature to low temperature quenching (generally defined as cooling γ′) have the form of ogdoadically-diced cubes, which have {100} cube plane interfaces with the γ matrix [4]. The schematic drawings of Figure 1 [4] show the γ′ particle shape following {100} or {111} planar sectioning. Figure 1(a) shows a perfect ogdoadically-diced cube on the {111} plane. Figure 1(b) shows the effect of the preferential growth along the [111] cube diagonal directions on the appearance of the sectioned γ′ particles. When the sectioning plane is [001], γ′ particles show 4-fold symmetry, on the other hand when the sectioning plane is {111} γ′ particles show 3-fold symmetry, Figure 1(b). In this study the above method was employed to study the crystallographic orientation of the γ grain fracture plane around crack initiation site for LCF samples tested at RT and elevated temperature. Finally, OIM was employed to confirm the results.

## Experimental Procedure

### Material and Microstructure

The material used in this investigation was an IN100 (PM) pancake forging. The composition is 12.4Cr, 18.5Co, 4.7Ti, 5.5Al, 3.2Mo, 0.8V and 0.07C (wt. %). A supersolvus heat treatment was employed and the resulting microstructure is shown in Figure 2. Other details of the processing information are proprietary. The average grain size is 30 μm with a range from 10 to 70 μm. Grain boundaries are delineated by primary irregular shaped γ′. Cooling γ′ particles are clearly visible in each γ grain. The stress ranges for $\sigma_{ys}$ and $\sigma_{UTS}$ at RT, 427°C and 704°C are shown in Table 2. Apparently, the $\sigma_{ys}$ is relatively constant from 427°C to 704°C.

Table 1. Fatigue Crack Propagation Plane Identification of Superalloys

| Author | Material | Temp. (°C) | da/dN (mm/cycle) | Plane ID | Comments |
|---|---|---|---|---|---|
| Vinvent & Remy [2] | Mar-M004 | RT<br>600 | $10^{-6}$ | (111)<br>(100) | Facet fracture close to threshold<br>Facet fracture close to threshold |
| King [4] | Astroloy | RT<br>RT | $>10^{-5}$<br>$<10^{-5}$ | (111)+(100)<br>(111) | Facet to striation transition<br>Facet fracture close to threshold |
| Sadananda & Shahinian [3] | Udmit 700 | RT<br>800 | $>10^{-4}$<br>$>10^{-4}$ | (100)<br>(100) | Facet to striation transition<br>Facet to striation transition |

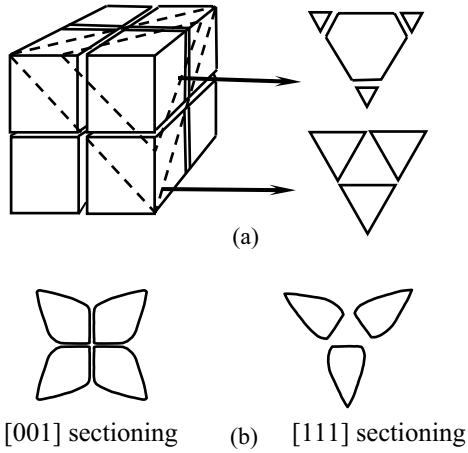


Figure 1. {111} Fracture surface facets: (a) sectioning of a perfect ogdoadically diced cube on {111} and (b) γ′ shape under {001} and {111} sectioning associated with an effect of preferential growth along [111] at vertices [4].

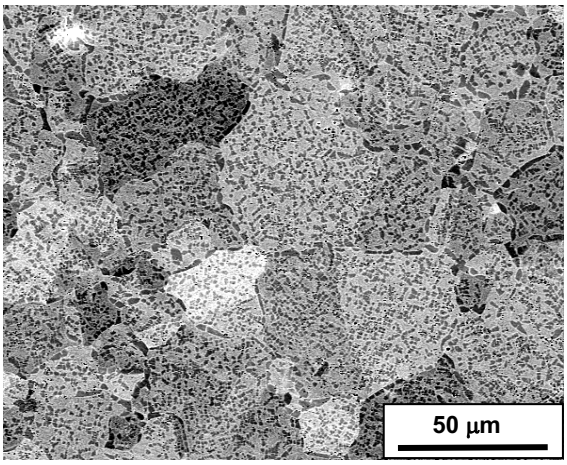


Figure 2. SEM back-scattered image showing microstructure of IN100 (PM).

LCF Testing and OIM

Nine cylindrical samples having a nominal gage diameter of 6.35 mm were employed for 538°C LCF testing. The axes of all the cylindrical samples were parallel to the circumferential direction of the forging. Flat dog bone samples used for RT testing have 5 mm gage width and 2 mm thickness. The flat surfaces of the samples are parallel to the forging plane with longitudinal axis parallel to the radial forging direction. Two dog bone samples were tested at ambient temperature. The sample surfaces were low stress ground and electropolished except as noted.

Identical fatigue testing conditions were employed at RT and 538°C. All testing at 538°C was conducted in air at 0.5 Hz under load control with a stress ratio of 0.05. The $\sigma_{max}$ was from 1000 - 1140 MPa, well beyond the yield strength, 880 - 960 MPa. The detail testing results at 538°C were given in [10].

To investigate fracture plane orientation under LCF conditions tested at RT, the flat dog bone Sample 01-981 was fatigued until fracture ($\sigma_{max}$ = 941 MPa, $N_f$ = 103,619 cycles). Flat dog bone Sample 01-986 ($\sigma_{max}$ = 950 MPa, N ~50,000 cycles) was fatigued and the test was interrupted when the maximum crack length was about 1 mm. The detail process was as following. Before fatigue testing one side of Sample 01-986 was roughly ground to introduce compressive residual stress to prevent crack initiation. As a result multiple cracks initiated only on the other side of the sample that was mechanically polished and monitored *in situ* by an infrared camera. A crack about 20-30 μm long was initially detected by the camera. When the maximum crack size of those initiated was about 1 mm in surface length the fatigue testing was interrupted. Totally, 14 cracks with lengths ranging from 47 to 1,074 μm were observed at the sample surface characterized using optical and scanning electron microscopy. Subsequently, the fatigued but not fractured sample was annealed in a vacuum furnace at 704°C (1300°F) for three hours to assist recovery of the microstructure. Finally, the sample surface was mechanically ground to remove a few microns of the plastically deformed layer and then was electropolished. All of these were aimed to improve back-scattered electron diffraction pattern quality in OIM scanning. The OIM scan was conducted in the region, which contained the longest crack of about 1 mm. To study the possible presence of micro-texture, OIM was also carried out on a cross section of the forging.

The OIM back-scattered electron detector was installed in a Leica 360 scanning electron microscope. The OIM operating parameters for all the samples were employed as follows: voltage 20 kV, probe current 7 nA, scanning step 0.6 μm and working distance 25 mm with sample tilted 70° to the incident electron beam.

Table 2. Yield and Tensile Strengths of IN100

| Strength (MPa) | RT | 427°C | 704°C |
|---|---|---|---|
| $\sigma_{ys}$ | 931- 960 | 877 - 944 | 886 - 939 |
| $\sigma_{UTS}$ | 1445 - 1483 | 1367 - 1408 | 1160 - 1188 |

Etching and Electropolishing

The fracture surfaces of fatigued sample 01-981 tested at RT were etched using waterless Kallings to reveal the cooling γ′ shape. The fracture surfaces of 538°C fatigued samples were electropolished to remove a bluish or grayish thin oxide layer about 2 or 3 μm thick, which formed during high temperature exposure. Electropolishing was conducted at 18 V and –50°C in the solution of 590 ml methanol, 350 ml 2-butanol and 60 ml hydroperchloric acid (60% concentrate) by moderate agitation. The sample was placed in the center of a circular stainless steel cathode with the fracture surface up. Following electropolishing, the fracture surface became shiny due to removal of the oxide layer. As a result, the cooling γ′ shape in γ grain matrix was revealed under SEM observation. Additionally, all OIM samples were also electropolished using the same electrolyte and polishing conditions.

**Results and Discussion**

Crystallographic Fracture Surfaces at RT

Low magnification SEM images showed a fatigue crack initiation region was located in the corner of the sample. Relatively high magnification images indicated that a fatigue crack originated from a large pore and propagated through a 70 μm grain. The fatigue crack initiation region of the fracture surface is very rough. A few 3-fold symmetrically arranged γ′ particles in the fracture plane (about 200 - 300 μm from the large pore) in Figures 3(a) and (b) clearly indicated that the fracture planes were {111}. Apparently, fracture occurred in two adjacent (111) planes, as shown in Figure 3(b), indicating more plastic deformation was required for microcrack propagation.

SEM images of a crack (about 500 μm long) among 14 cracks on the surface of sample 01-986 fatigued at RT are shown in Figure 4. Apparently, the fracture planes of the LCF crack are {111} types since crack paths were parallel to the slip bands. In Figure 4(b) crack branching (indicated by an arrow) formed a 60° triangle indicating a [111] grain normal. Furthermore, it was evident in both images that multiple slip system activation occurred. It is well documented that for microstructural small crack growth at RT the crack path is typically along slip bands [1].

Crystallographic Fracture Surfaces at 538°C

The fatigue crack initiation sites of all nine samples were defect related, either pores or non-metallic inclusions. In eight of nine samples the fatigue crack initiated from defects on or near the sample surface, thus the micro-crack growth formed thumbnail cracks. The fracture surfaces around crack initiation sites that are denoted by dotted lines in Figure 5 are faceted. The faceted area extended to approximately 100 - 150 μm independent of stress

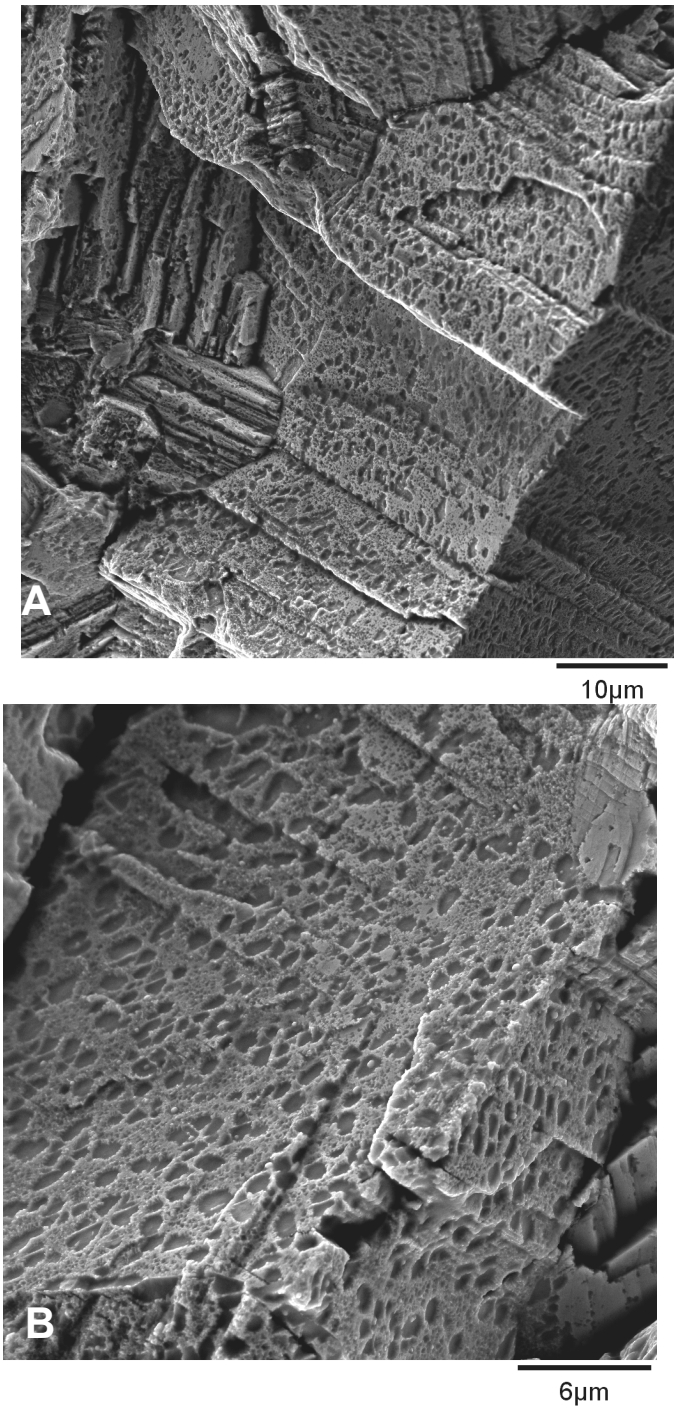


Figure 3. SEM images showing {111} fracture planes (close to an initiation site): (a) a low magnification image and (b) two {111} fracture planes.

level. Recall the grain size is about 30 μm in average. Thus, the microcrack growth is about three or five times the average grain size. Furthermore, the fatigue crack initiation regions (semicircular or circular) of all nine samples are macroscopically perpendicular to the loading axis.

Compared to RT fatigued samples, the fatigue crack initiation regions on the fracture surfaces tested at 538°C are relatively smooth, indicating that crack initiation probably did not occur on {111} type planes. A similar observation of the flatness of fatigue crack initiation regions was also reported by Albrecht [8]. His LCF tests of U720 LI were conducted at 600°C. Different cooling rates produced grain sizes of 22, 65, 130 and 420 μm. SEM images showed that the fracture surfaces, within the range of microcrack propagation, were quite flat on all the samples, which had significant different grain sizes.

In our study corresponding SEM images were taken prior to and following electropolishing of the fracture surfaces. The fracture surface following electropolishing was even smoother than prior to electropolishing due to the disappearance of numerous ridgelines. Since electropolishing only removed a 1 - 2 μm thick-layer from the sample surface, we estimated that the step heights corresponding to the ridgeline locations were no higher than 1 - 2 μm. If the fracture surface around the initiation site is flat, then microtexture exists in the local grains. In a 65 x 85 μm flat crack initiation region, Figure 6(a), the cubic γ′ shape in the fracture surface revealed that the majority of grains (totally about 15 grains) were close to {001} orientation (with rotation freedom about [001]). Figure 6(b), enlargement of Figure 6(a), indicated that the γ′ particles were ogdoadical cubes. Additionally, no secondary cracking was detectable in the initiation regions.

OIM Results

Although using γ′ shape to identify the fracture plane orientation is a convenient and practical method, some disadvantages exist. In general, only a few γ′ particles have perfect ogdoadic cubic shapes in a grain. In addition, distinguishing (001) from (110) is difficult just by studying the γ′ shape on the fracture plane. Thus, the conclusion obtained above must be confirmed by accurate 3D grain orientation determination or OIM. A back-scattered SEM image of a crack (about 1 mm in total length) and surrounding microstructure of Sample 01-986 is shown in Figure 7(a). The corresponding [001] inverse pole figure (IPF) map with an orientation key attached is shown in Figure 7(b). Since color printing in manuscripts for this Symposium will not be available, grains outlined in Figures 7(a) and (b) are labeled R, G and B indicating [001], [110], and [111] orientation, respectively. Comparing the corresponding grains in Figures 7(a) and (b), apparently, grains with [100] or [111] orientation resulted in different γ′ particle shape and morphology. However, the use of γ′ particle shape and morphology can't distinguish [100] from [110] since a [110] grain outlined and labeled G does show apparent 4-fold symmetrical γ′ particles, indicated by an arrow in Figure 7(a). Fortunately, {110} fracture doesn't seem to occur for this class of alloys.

Presence of Microtexture

The following facts and results could be summarized from the 538°C LCF testing. All the sample axes were machined to be parallel to the circumferential direction of the forging; each fatigue crack initiation or faceted region was perpendicular to the loading axis; the faceted micro-crack propagation region is relatively flat and majority of the grains in the region have {001} orientation. These facts seem to imply that a {001} microtexture was present in the cross section of the forging. Figure 8 is [001] IPF map of the microstructure of a cross section of the IN100 forging. The grains having [001] orientation were hatched. The OIM scanned region is about 280 x 148 μm. Although no strong indication of bulk texture is present in the entire microstructure, a few grains in the central part of the sample have orientations close to {001}. If a large defect is present in the hatched regions and the loading axis is close to [001] direction, a critical crack size for crack initiation at elevated temperature will be attained. In other words a few neighboring grains with similar orientation are acting as one large grain in the fatigue crack initiation process.

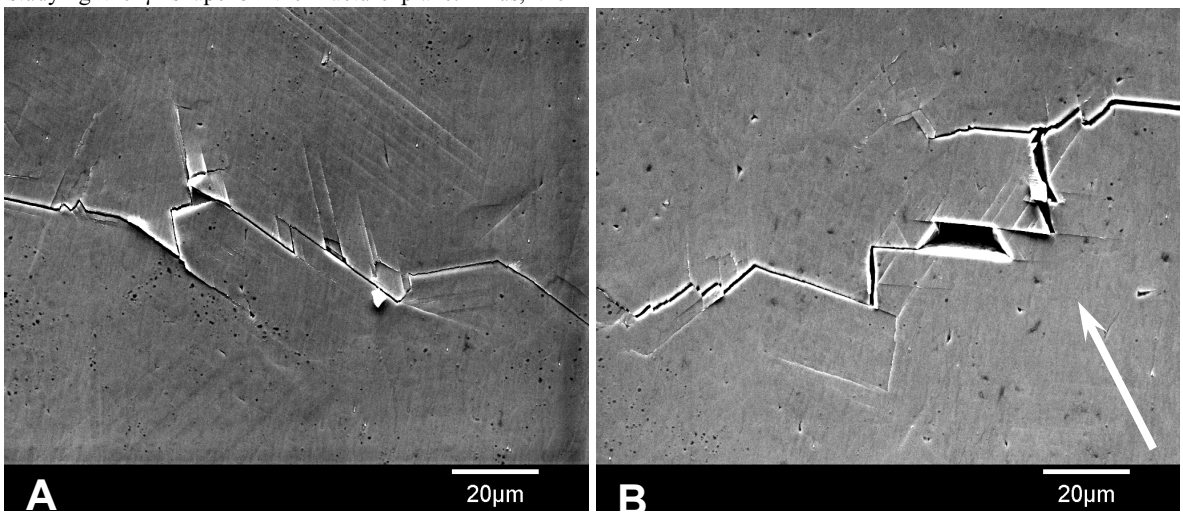


Figure 4. SEM images showing a fatigue crack on the surface of the dog bone sample 01-986 tested at RT: (A) fatigue crack parallel to the slip line and (B) a defect and fatigue crack branches parallel to slip lines. The arrow shows crack branching forming a 60° triangle indicating a [111] grain normal.

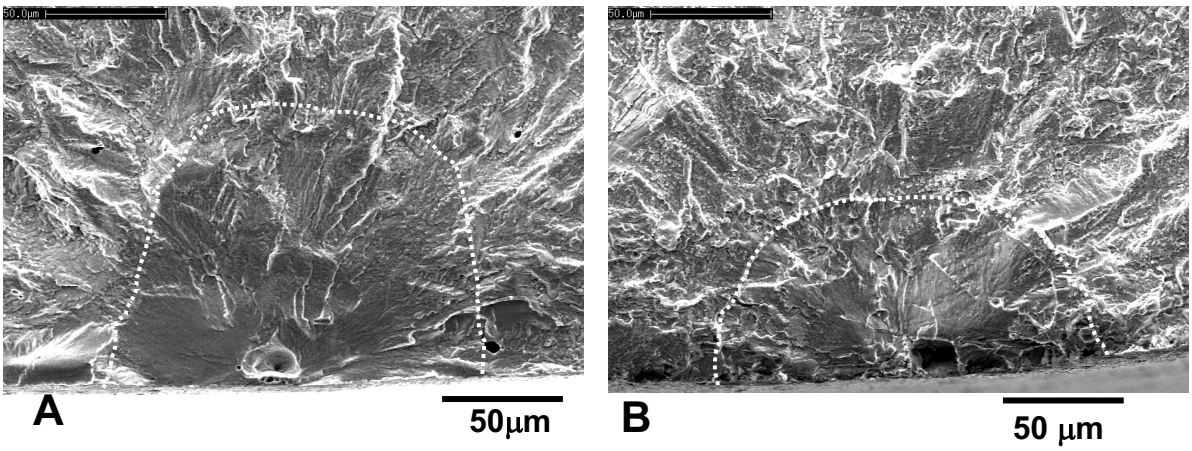


Figure 5. SEM images showed the fracture surfaces around crack initiation sites are faceted, (A) Sample 01-491 and (B) Sample 01-486.

Multiple Crack Initiation

It is well documented that for nickel-base superalloys the fatigue crack initiation sites are always multiple when the maximum stress level is close or beyond the material yield strength [1, 11]. The question is, which crack will propagate faster (some times crack linkage occurs) and become the dominant crack that is responsible for the final fracture? It is known that the fluctuation of the crack growth resistance for the microstructurally small crack is often attributed to the retardation of crack growth by grain boundaries [1]. Recent detailed research [12] on the boundary retardation of small crack growth demonstrated that the twist and tilt angles of the crack plane deflection in the grain boundary are the key factors that control the path and growth rate of a small crack. Results from this study suggested that among the multiple initiated cracks under LCF conditions, the crack associated with a local texture that has a favorable orientation to the loading axis very likely develops into a dominant crack.

## Conclusions

Crystallographic, faceted fracture around fatigue crack initiation sites was observed under LCF testing condition at RT and elevated temperature. However, the fatigue micro-crack propagation occurs on the {111} plane at ambient temperature and on the {001} plane at elevated temperature. The different fracture planes result in different initiation region appearance on the fracture surface: flat at elevated temperature and rough at RT. This appearance indicated that micro crack propagation was controlled by the temperature dependent dominant deformation modes.

The crack nucleation in pores and nonmetallic inclusions under LCF conditions of IN100 is dominant at RT and elevated temperature [1, 9-11]. LCF life depends on fatigue crack initiation life and microcrack propagation life. The crucial parameters, which affect the LCF life of this class alloy, are defect content, grain size and local grain orientations. The results of this work indicate that the promotion of crack initiation and propagation requires the following conditions: coincidence of a critical size defect and a large grain or a local texture that has a favorable orientation to the loading axis. The increase of LCF resistance of the microstructure not only requires uniform grain size but also requires a random distribution of grain orientations.

## Acknowledgements

The authors are grateful to B. Grubb and P. Blosser (UDRI) for conducting fatigue tests. Thanks are also due to R. Lewis (UES) for his work at etching and electropolishing samples. Financial support for Li and Ashbaugh was from the project 'Life Prediction Methodologies for Aerospace Materials' F33615-98-C-5214.

## References

**1.** Luo J. & P. Bowen, 'Small & long fatigue crack growth behavior of a PM Ni-based superalloy, Udimet 720', *Inter. J. fat.,* **26** (2004), p113-124.

**2.** Vincent, J. N. and Remy, L., 'Temperature dependence of the pseudo-cleavage mechanism in the threshold regime of a superalloy'. *Fatigue Threshold*, eds., Blacklund, J. et al, p.441-454.

3 Sadananda, K. and Shahinian, P. 'Analysis of crystallographic high temperature fatigue crack growth in a nickel-base alloy'. *Met. Trans*. **12A** (1981)**,** p343-351.

4. King, J. E. 'Crystallographic fatigue crack growth in Nimonic API', *Fatigue of Eng. Mater. & Structures*. **4** (1981), No.4, p311-320.

5. Purushothaman, S. and Tien, J. K. 'Slow crystallographic fatigue crack growth in a nickel-base alloy', *Metal. Trans A*, **9A**(1978), p351-355.

6. Davidson D. L. and Chan, K. S, 'The crystallography of fatigue crack initiation in coarse grained Astroloy at 20C', *Acta Metall.* **37**(1989), No.4, p1089-1097.

7. Antolovich S. D. and Rosa, E. 'Low cycle fatigue of Rene 77 at elevated temperatures', *Mater. Sci. & Eng.,* **47**(1981), p47-57.
8. Albrecht J. 'Comparing fatigue behavior of titanium and nickel-based alloys', *Mater. Sci. & Eng.* **A263** (1991), P176-186.
9. Hyzak, J.M. and Bernstein, I. M (1982), 'The effect of defects on the fatigue crack initiation process in two P/M super alloys: part I. Fatigue origins and Part II surface-subsurface transition', *Metall., Trans, A*, p.33 (part I) and p.45 (part II).
10. K. Li, N. E. Ashbaugh and A.H. Rosenberger (2002), 'Effects of defects on crack initiation of IN100 (P/M) under low cycle fatigue conditions', *Fatigue 2002, Proceedings of the 8th International fatigue Conference, Stockholm, Sweden, June 2002,* editor, A. F. Blom, **2**. p.851-858.
11. Pang. H. T. and Reed P.A.S, 'Fatigue crack initiation & short crack growth in nickel-base turbine disc alloys-the effects of microstructure & operating parameters' *Inter. J. Fat.,* 25 (2003), p1089-1099.
12. Zhai T, Wilkinson A. J. & Martin J. W, A, 'Crystallograpphic mechanism for fatigue crack propagation through grain boundaries'. *Acta Mater.* 2000; 48, p4917-27.

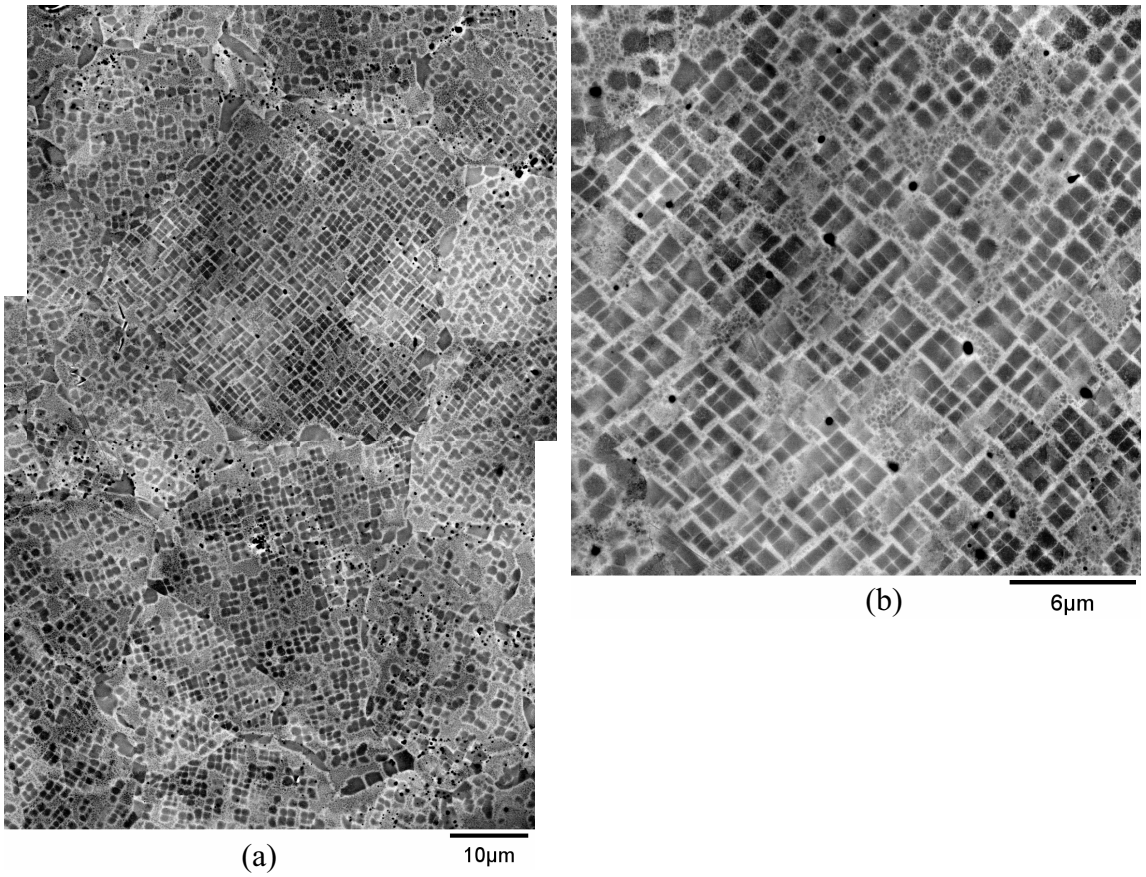


Figure 6. SEM images showing {001} fracture plane tested at 538°C: (a) most γ grains having {001} orientation and (b) enlargement of a γ grain.


(a)

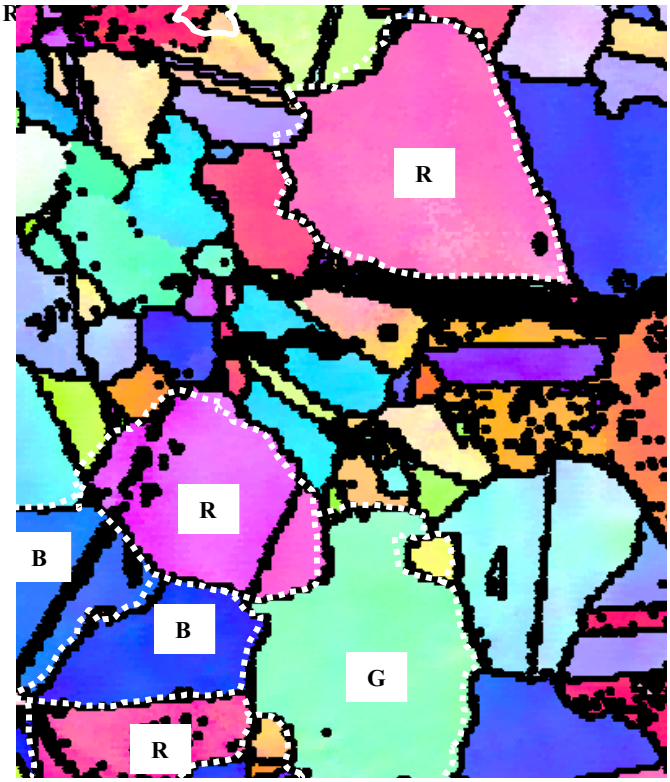


(b)

Figure 7. An SEM image (a) and a corresponding OIM [001] IPF map (b) are shown. The capital letters in outlined grains (b) indicate grain orientation: R = [001], B = [111] and G = [110]. The arrow in (a) points to an apparent 4-fold symmetric γ′ particles in a [110] grain. Note that the apparent symmetry of the 4-fold γ′ shape is not always easy to determine.

Orientation Key

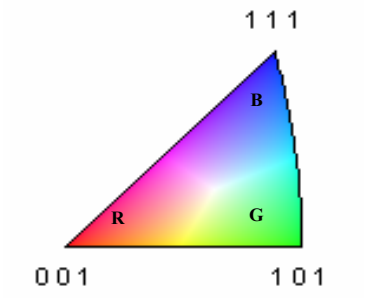


Figure 8. OIM [001] IPF map; grains having [001] orientation are hatched.